

1 **Along arc heterogeneity in local seismicity across**
2 **the Lesser Antilles subduction zone from a dense**
3 **ocean-bottom seismometer network**

4
5
6 Lidong Bie*, Andreas Rietbrock*, Stephen Hicks, Robert Allen, Jon Blundy, Valerie
7 Clouard, Jenny Collier, Jon Davidson, Thomas Garth, Saskia Goes, Nick Harmon, Tim
8 Henstock, Jeroen van Hunen, Mike Kendall, Frank Krüger, Lloyd Lynch, Colin
9 Macpherson, Richard Robertson, Kate Rychert, Stephen Tait, Jamie Wilkinson, Marjorie
10 Wilson

11
12 Corresponding author: Lidong Bie (l.bie@liv.ac.uk)

13 Geophysical Institute, Karlsruhe Institute of Technology, Germany

14 *Also at Department of Earth Ocean & Ecological Sciences, University of Liverpool, UK

17 **ABSTRACT**

18

19 The Lesser Antilles arc is only one of two subduction zones where slow-spreading
20 Atlantic lithosphere is consumed. Slow-spreading may result in the Atlantic lithosphere
21 being more pervasively and heterogeneously hydrated than fast-spreading Pacific
22 lithosphere, thus affecting the flux of fluids into the deep mantle. Understanding the
23 distribution of seismicity can help unravel the effect of fluids on geodynamic and
24 seismogenic processes. However, a detailed view of local seismicity across the whole
25 Lesser Antilles subduction zone is lacking. Using a temporary ocean-bottom seismic
26 network we invert for hypocentres and 1-D velocity model. A systematic search yields a
27 27 km thick crust, reflecting average arc and back-arc structure. We find abundant
28 intraslab seismicity beneath Martinique and Dominica, which may relate to the
29 subducted Marathon/Mercurius Fracture Zones. Pervasive seismicity in the cold mantle
30 wedge corner and thrust seismicity deep on the subducting plate interface suggest an
31 unusually wide megathrust seismogenic zone reaching ~65 km depth. Our results
32 provide an excellent framework for future understanding of regional seismic hazard in
33 eastern Caribbean and the volatile cycling beneath the Lesser Antilles arc.

34

35 **INTRODUCTION**

36

37 Subduction zones are key centers of mass transfer in the Earth, where the lithosphere
38 and its cargo of volatiles are recycled back into the Earth's interior. In contrast to Pacific
39 subduction margins, where fast-spreading lithosphere is consumed, subduction of slow-
40 spreading lithosphere such as that formed in the Atlantic should result in a more
41 heterogeneous distribution and possibly higher amount of fluids entering the subduction
42 zone (Escartín *et al.*, 2008). The Lesser Antilles subduction zone in Eastern Caribbean
43 is a global end-member in that the subducting plate is relatively old (~80 Myr) but yet
44 subducts very slowly at ~19 mm/yr (DeMets *et al.*, 2010), and it is one of two zones
45 where the slow-spreading Atlantic oceanic lithosphere is consumed. Along-arc changes
46 in fluid flux might affect the distribution and character of seismicity and associated
47 volcanism. For example, pore fluids within subducting sediments may affect the seismic

48 character of subduction megathrusts (Heuret *et al.*, 2012), and intermediate-depth
49 intraslab earthquakes are probably caused by dehydration embrittlement (e.g., Abers *et*
50 *al.*, 2006). A coherent view of local seismicity throughout the Lesser Antilles subduction
51 zone is thus important for understanding fluid pathways and their influence on seismicity
52 as well as for improving seismic hazard assessment.

53

54 Available measurements for the Lesser Antilles arc indicate that subduction parameters,
55 such as slab dip (Wadge and Shepherd, 1984), Wadati-Benioff zone thickness, and slab
56 geometry (Bie *et al.*, 2017), vary significantly along the Lesser Antilles subduction zone.
57 Changes in slab dip as well as thickness and depth of the Wadati-Benioff zone near 15°
58 latitude have been attributed to either the subduction of fracture zones (Schlaphorst *et*
59 *al.*, 2016; Bie *et al.*, 2017) or a slab tear and gap wide enough to allow mantle flow
60 through (e.g., van Benthem *et al.*, 2013; Harris *et al.*, 2018; Schlaphorst *et al.*, 2017). It
61 is debated whether these changes in slab properties mark the location of the current
62 North-South American plate boundary (Bie *et al.* 2017) or this boundary is located
63 further north as suggested by plate reconstructions (Bird, 2003)

64

65 There have been several studies that characterise Lesser Antilles seismicity
66 teleseismically (e.g., McCann and Sykes, 1984; Hayes *et al.*, 2013) as well as studies of
67 local earthquakes for some parts of the arc (e.g., Dorel *et al.*, 1981; Paulatto *et al.*,
68 2017; Ruiz *et al.*, 2013). These studies found higher rates of seismicity in the northern
69 part of the Lesser Antilles subduction zone (14-18° N) than in the south, both in terms of
70 small events and in historical records (e.g., McCann and Sykes, 1984; Hayes *et al.*,
71 2013). Two historic M>8, presumably thrust, earthquakes have been documented in the
72 northern Lesser Antilles (e.g., Feuillet *et al.*, 2011). However, the strength of plate
73 interface coupling and its variation along strike remain uncertain due to sparse GPS
74 observations and slow convergence (e.g., López *et al.*, 2006). Local studies have
75 detected earthquakes in the fore-arc corner of the mantle wedge (Ruiz *et al.*, 2013,
76 Laigle *et al.*, 2013), something that has only been seen in a few subduction zones
77 worldwide (e.g., Halpaap *et al.*, 2019).

78

79 No recent efforts have systematically characterised the distribution of small-magnitude
80 seismicity along the full extent of the Lesser Antilles plate margin. The inherent nature
81 of oceanic subduction zones means that onshore permanent seismometer networks
82 have limited coverage and aperture, making it difficult to accurately locate small-to-
83 moderate magnitude earthquakes in the back- and fore-arc. Furthermore, there is no
84 well-constrained 1-D velocity model for the Lesser Antilles, which adds to earthquake
85 location uncertainties. As part of our Volatiles Recycling in the Lesser Antilles (VoiLA)
86 project (Goes *et al.*, 2019), we deployed a network of 34 broadband ocean-bottom
87 seismometers (OBS) in 2016, which were recording for 14 months. We use this OBS
88 data, complemented by recordings from permanent and temporal land stations, to jointly
89 invert for 1-D P- and S-wave velocity models, earthquake locations and station
90 corrections. Our study provides the first unified reference velocity model for the Lesser
91 Antilles region, useful for the routine location of earthquakes in the area. The recorded
92 seismicity provides the opportunity to understand the fore- and back-arc structure,
93 thermal structure in the mantle wedge, and deformation mechanisms at intermediate
94 depths in the subducted slab.

95

96 **SEISMIC EXPERIMENT AND DATA**

97

98 In March 2016, a network of 34 broadband OBS was installed across the fore- and
99 back-arc regions of the Lesser Antilles subduction zone (Figure 1). The OBS were
100 retrieved in May 2017. Two stations encountered hardware failures, leaving 32 stations
101 with useable data (Goes *et al.*, 2019). In addition to our temporal OBS observations, we
102 collected seismic data from existing permanent stations as archived by IRIS DMC
103 (Figure S1). We also filled the gap in permanent stations along the southern end of the
104 arc by deploying eight temporary stations in January 2017.

105

106 Multi-channel seismic surveys were also made during expedition JC149 in April 2017.
107 Shooting occurred along eight lines, most of which were in a north-south direction along
108 the arc and in the back-arc, with two lines taken perpendicular to the arc in the north of
109 the subduction zone (Figure S1). These active-source data help to constrain the shallow

110 velocity structure of the subduction zone, an area poorly resolved in many passive-
111 source tomographic inversions.

112

113 **MINIMUM 1-D VELOCITY MODEL**

114 **Initial Catalogue**

115 By collating the events reported by various agencies, we created an initial earthquake
116 catalogue for manual picking P- and S-wave onset times. Our initial catalogue includes
117 events from the online bulletin of the International Seismological Centre (ISC), the
118 Martinique Seismic and Volcano Observatory, and the Seismological Research Centre
119 of the University of West Indies (hereafter, UWI-SRC). We also detected additional
120 events using an automated short-term average ratio/long-term average (STA/LTA)
121 triggering algorithm (Nippres *et al.*, 2010) on vertical components of the ocean-bottom
122 stations and performed an iterative event association procedure following Rietbrock *et*
123 *al.* (2012). We then manually read P- and S-wave onset times from these potential
124 events on the ocean-bottom stations and all available onshore stations using the
125 Seismic Data Explorer (SDX) software (<http://doree.esc.liv.ac.uk:8080/sdx>). Based on
126 onset time uncertainties, we assigned each observation a weight as follows: Weight 0
127 (<0.1 s); Weight 1 (0.1-0.2 s); Weight 2 (0.2–0.5 s); Weight 3 (0.5–0.8 s); Weight 4 (>0.8
128 s). Initial locations were computed using the IASP91 1-D reference velocity model
129 (Kennett and Engdahl, 1991). This workflow resulted in a total of 502 confirmed
130 earthquakes.

131

132 We computed local magnitudes (M_L) for all events in our catalogue. Maximum
133 amplitudes were taken from instrument-corrected waveforms, which were simulated to a
134 Wood-Anderson seismometer. We took the largest peak-to-peak amplitude from all
135 station components within a time window starting at the picked P-wave arrival and
136 ending at a time window 30 seconds after the theoretical slowest travelling L_g wave
137 (assuming a minimum L_g velocity of 3.0 km/s). We computed amplitudes for traces that
138 had a root-mean square (RMS) signal-to-noise ratio greater than 3 to ensure that
139 amplitude measurements were not contaminated by ocean microseism noise. We
140 computed station magnitudes based on the M_L scale for central California (Bakun and

141 Joyner, 1984). Overall event magnitudes were then calculated based on a 25%
142 trimmed-mean of station magnitudes to reject outliers. We found that station amplitudes
143 measured at both ocean-bottom and onshore stations fit well the M_L scale over a range
144 of hypocentral distance (see Figure S2 for examples). Regression analysis shows that
145 our computed event local magnitudes correlate well with moment magnitude estimates
146 for $M_w > 4.5$ events (Figure S3a), and with local duration magnitudes (M_d) for smaller
147 events (Figure S3b).

148

149 **1-D minimum velocity model inversion**

150 Out of 502 manually picked events, we select a high-quality subset of 265 events with a
151 maximum azimuthal gap of less than 180° , and with at least 20 P-wave and 5 S-wave
152 arrivals. The subset consists of $\sim 10,600$ P-wave and $\sim 8,200$ S-wave arrivals for the
153 simultaneous inversion of a 1-D layered velocity model, earthquake location and station
154 corrections using the VELEST software (Kissling *et al.*, 1994).

155

156 The travel-time of a seismic wave is dependent on both the hypocentre parameters
157 (origin time and location) and seismic velocity structure of the medium that the ray-path
158 travels through. Such a coupled hypocentre-velocity problem can be solved by ray-
159 tracing and updating the velocity model and hypocentre simultaneously (Kissling *et al.*,
160 1988; Eberhart-Phillips, 1990; Thurber, 1992). We conducted the simultaneous
161 inversion using the VELEST software by Kissling *et al.* (1994). VELEST requires that all
162 stations must be in the same velocity layer. In this study, the deepest OBS station sits
163 ~ 5 km below sea level and the greatest land station elevation is ~ 1.4 km, making it
164 impractical to set a model with a 7 km thick uppermost layer. Instead, we followed the
165 strategy of Husen *et al.* (1999) and Hicks *et al.* (2014) by setting station elevations to
166 zero and allowing station delay terms to absorb systematic travel-time errors due to
167 elevation differences, as well as possible lateral heterogeneity in subsurface structure.

168

169 In addition to passive seismic data, we included 63 active shots from the seven shot
170 lines (Figure 1) in order to better constrain seismic velocities at shallow depth,
171 especially in the back-arc region, where few earthquakes with shallow hypocentral

172 depth occur. For each shot line, the gap between our selected neighbouring shots is
173 roughly 15 km. The arrival times were manually picked on 22 OBS stations that record
174 part of the 63 shots. The arrival times were corrected to subtract travel-time through the
175 sea-water-column to be consistent with setting the station depth to sea level.

176

177 A robust initial starting velocity model is required as *a priori* information. We chose the
178 velocity model computed by Raffaele (2011) as our starting model. Given that this
179 model only extends to 30 km depth, we extended the starting model to a depth of 200
180 km by merging it with the IASP91 velocity model below 30 km depth. To search for the
181 best-fitting minimum 1-D model, ensuring that we are not fitting local misfit minima, we
182 perturbed the starting model randomly within ± 0.5 km/s for all layers, resulting in 1000
183 different synthetic starting models. The degree of convergence of the final velocity
184 models from the 1000 inversions with different starting models is the first evidence of
185 how robust the best-fitting model is. The velocity model that gives the minimum root-
186 mean-square (RMS) misfit was taken as the optimal minimum 1-D velocity model.

187

188 We first invert for P-wave velocity model, using P-wave arrivals only. The best 10
189 velocity models with the smallest RMS misfit converge very well. We notice an increase
190 of velocity from 7.0 to 7.7 km/s at a depth of 27 km. To test whether the Moho depth can
191 be constrained by our datasets, we manually alter the starting model by varying the
192 depth to the bottom of the third layer from 21 to 37 km, in 2 km increments (Figure 2a).
193 Then the inversion is conducted in the same way as described above by generating
194 1000 variations of starting models for each Moho depth scenario and searching for the
195 best model that gives minimum RMS. We then plotted the minimum RMS values versus
196 the prescribed Moho depths, and the comparison shows a preferred average Moho
197 depth of 27 km (Figure 2c).

198

199 After obtaining the best P-wave velocity model and optimal Moho depth, we
200 subsequently inverted for S-wave velocity model using P- and S-wave arrival times.
201 Similarly, 1000 variations of S-wave starting velocity model are generated, based on the
202 P-wave velocity model and average v_p/v_s ratio derived from Wadati analysis. Due to the

203 trade-off between station corrections and the top layer velocity, we chose not to fix the
204 top layer P-wave velocity as derived from the inversion.

205

206 **Characteristics of Minimum 1-D Velocity Model**

207 Tests with a range of starting models with various Moho dept (Figure 2a) result in the
208 final minimum 1-D velocity model shown in Figure 2b. The best-fitting 1-D minimum
209 velocity model comprises two layers of upper-plate crust underlying a top sedimentary
210 layer. The estimated crustal P-wave velocity increases from 4.3 km/s at shallow depth
211 to 7.7 km/s at 27 km depth. Affected by mostly near-vertical ray-paths, the uppermost
212 crustal layer velocity is less well constrained, shown by poor convergence of the 10 best
213 models, implying strong spatial variation of uppermost crustal velocity. This does not
214 influence the final earthquake locations however, as our analysis of locations
215 corresponding to the best 10 velocity models show a small average shift of <100 meters
216 in all directions. The average velocities for the two main crustal layers are 6.3 km/s and
217 7.0 km/s, consistent with those determined by Boynton *et al.* (1979) for the island arc.
218 Our systematic search with varying crustal thickness yields a minimum misfit when the
219 Moho depth is 27 km (Figure 2c). Crustal thicknesses derived by González *et al.* (2018)
220 from surface wave and receiver function analysis under 19 land stations along the arc
221 vary from 21 km beneath St Lucia to 33 km beneath Grenada in the south, with an
222 average of 26 km (Figure 2c), which is similar to our model value even though this
223 constitutes an average across the margin. Between 27 km and 200 km depth, the P-
224 wave velocity (v_p) and S-wave velocity (v_s) increasing steadily to 8.7 km/s and 4.9 km/s,
225 respectively, fits the observations (Table S1).

226

227 Station corrections are incorporated to compensate 3-D heterogeneity of near-surface
228 velocity and station elevations. Station corrections for v_p are generally smaller than 0.5
229 s, while for v_s , the station corrections are larger but mostly below 1.0 s (Figure 3). There
230 are some systematic patterns, including positive corrections (i.e., thicker or slower crust)
231 north and negative corrections south of reference station DP05 near Martinique in the
232 central arc, as well as a linear correlation between station elevation and correction for

233 the OBS (Figure S4). Based on active source imaging (Allen *et al.*, 2019), our preferred
234 interpretation is a systematic variation in crustal thickness from north to south.

235

236 **OVERALL CHARACTERISTICS OF LA SEISMICITY AND SUBDUCTION** 237 **GEOMETRY**

238

239 The best-fitting velocity model is used to relocate the original 502 manually-picked
240 events. We conducted hypocentre location stability tests by randomly perturbing
241 hypocentres ± 7.5 -12.5 km in 3-D, then relocating using the best-fitting 1-D velocity
242 model (Figure 2b). When the azimuthal gap is less than $\sim 270^\circ$, the earthquakes
243 generally relocate back to their original positions (Figure 4a), with a standard deviation
244 of 0.21, 0.17, and 0.77 km for latitude, longitude and depth, respectively (Figure 4b). In
245 addition to the azimuthal gap, we retained events that were relocated within 5 km depth
246 variation from the original position. Strict filtering after hypocentre location stability tests
247 resulted in 378 well-relocated events (Figure 5).

248

249 Although our observation period is short, the relocated seismicity exhibits a higher rate
250 in the northern part of the subduction zone than in the south (Figure 5 and 6), consistent
251 with previous studies (e.g., Bie *et al.*, 2017). Sparse seismicity is observed in the forearc
252 region within 50 km distance from the trench. However, station coverage close to the
253 trench in the outer forearc is very limited, so detection and location accuracy here is
254 reduced. Most seismicity beneath the outer forearc is found in the north, where the
255 forearc is less wide, and OBS stations were closer to the trench. We note that more
256 smaller earthquakes may be found using template-matching techniques (e.g., Zhu *et al.*,
257 2019). Here, we focussed on the larger events with robust arrival time determination,
258 particularly for the generation of a well-constrained 1-D seismic velocity, with less
259 emphasis on the evolution of seismicity in time and space.

260

261 Seismicity extends from the shallow upper crust of the overriding plate to intermediate
262 depths of 180 km in the central slab (Figure 5). The distribution of seismicity with depth
263 displays two peaks (see inset to Figure 5). Shallow seismicity increases with depth and

264 reaches its first peak at ~25 km, stays relatively high until there is a sharp reduction
265 below ~60 km depth. At depths greater than ~80 km, seismicity increases again to
266 depth of 170 km. The shallow peak comprises events in the overlying arc crust, and
267 between about 25 and 60 km depth, events along the plate interface and in the mantle
268 wedge corner. The deep peak consists of events within the subducting slab. The depth
269 ranges of these peaks are similar to those that Paulatto *et al.* (2017) identified below
270 Martinique, who proposed that the peaks in mantle wedge and slab seismicity are
271 associated with slab dehydration around 40 and 150 km depth. In Section 5 we discuss
272 the seismicity in each part of the system in detail.

273
274 Our catalogue of regional seismicity provides new constraints on slab geometry. As
275 shown in Figure 5, the seismicity distribution in this study does not agree well with the
276 global Slab2 plate geometry model (Hayes *et al.*, 2018). The slab surface in Slab2 is up
277 to 70 km shallower at depth of 180 km. Our seismicity is consistent with the
278 teleseismically-constrained slab geometry of Bie *et al.* (2017) to ~80 km depth, while
279 beyond that, seismicity in our study suggests a slightly steeper slab (profiles B-B', C-C',
280 and D-D' in Figure S5). We thus integrated the local seismicity in this study with the
281 global datasets used in Bie *et al.* (2017) and constructed a refined slab geometry
282 (Figure 5). How the large difference in slab geometry affects geodynamic modelling and
283 seismic hazard estimation will be a subject of a planned future study.

284

285 **DISCUSSION**

286

287 **Earthquakes in the Overriding Plate**

288 The shallow events lie in the overriding upper plate, reflecting fault failures in the fore-
289 arc and/or are related to volcanic structures along the arc. Profile A-A' shows a cluster
290 of events ~100 km westward of the trench at 14-25 km depth. These events are mostly
291 aftershocks of the M_w 5.7 thrust earthquake on 17 April 2017. The trenchward-dipping
292 alignment of the cluster may indicate failure of a back-thrust fault bounding the western
293 edge of the accretionary prism. A similar cluster can be found ~150 km west of the
294 trench in profile B-B'. It is unclear whether this cluster on B-B' was on splay thrusts or

295 back-thrusts, given no clear alignment is shown and the relatively large RMS misfit
296 values.

297

298 Profile B-B' shows another cluster of shallow seismicity in line with the volcanic arc,
299 between Guadeloupe and Dominica. This seismicity can be divided into two sequences.
300 The first in 2016 starts with M_L 4.5 and M_L 4.1 events on 12 April, and lacks a clear
301 subsequent aftershock sequence. The second sequence swarm started in April 2017
302 denoted by a M_L 3.5 earthquake (Table S2). Previously on 21 November 2004, this area
303 experienced a M_w 6.3 normal fault earthquake on the Roseau fault, which bounds the
304 western side of the Les Saintes Graben between Guadeloupe and Dominica (Bazin *et*
305 *al.*, 2010). The mainshock was followed by a long-lasting aftershock sequence on the
306 Roseau Fault and a short-lived aftershock sequence on the smaller antithetic normal
307 faults. Bazin *et al.* (2010) attributed the long-lasting aftershock sequence on the Roseau
308 fault to this region being strongly faulted and filled with fluids, as inferred from a low v_p
309 anomaly and a high v_p/v_s ratio, while for the short duration aftershock sequence, fluid
310 was less involved. This interpretation of high fluid content is consistent with our
311 observation of occasional swarm activity in this region.

312

313 Below Tobago, in the southern fore-arc, a sequence of aftershocks followed the M_w 5.9
314 strike-slip earthquake on 6 December 2016 (profile E-E' of Figure 5). Although, we
315 expected these to be upper plate events, the aftershocks were relocated to ~60 km
316 depth. A M_w 6.1 earthquake with a similar faulting mechanism occurred on 2 April 1997
317 at 45 km depth (NEIC), preceding a larger M_w 6.7 normal fault earthquake on 22 April
318 1997 at a much shallower depth of 5-15 km (NEIC). The GCMT focal mechanism for the
319 2016 event suggests either sinistral strike-slip on an E-W striking sub-vertical (dip 67°)
320 fault plane, or dextral strike-slip rupture on a near-vertical (80° dip) N-S striking fault
321 (Figure 6). This mechanism is not consistent with the current active E-W dextral
322 shearing across the Caribbean-South American plate boundary zone (e.g., Weber *et al.*,
323 2015). These strike-slip events lie anomalously deep beneath the fore-arc, and the 2016
324 cluster is close to the top of the subducting slab (profile E-E' of Figure 5). A likely

325 explanation is that the 2016 and 1997 strike-slip events ruptured structures within the
326 down-going oceanic crust.

327

328 **Mantle Wedge Seismicity**

329 In addition to shallow upper crust activity, seismicity in the overriding plate appears in
330 the mantle wedge corner above ~65 km depth and reaches into the lower crust (profiles
331 in Figure 5), consistent with Ruiz *et al.* (2013) and Laigle *et al.* (2013). Seismicity in the
332 mantle-wedge corner has implications for the thermal structure of the mantle wedge. It
333 is normally assumed that the stable-unstable sliding transition in oceanic mantle occurs
334 at temperatures of ~600°C (e.g., McKenzie *et al.*, 2005). By constructing an
335 approximate curve delineating the wedge-shaped mantle corner seismicity, we found
336 that the inferred transition consistently intersects the slab (red curve constrained by
337 seismicity in Figure 5 profiles) at ~65 km depth across the subduction zone. In contrast
338 to profiles in the north, the lack of mantle wedge seismicity in the EE' profile suggests
339 that the mantle wedge temperature is different from north to south.

340

341 Mantle-wedge corner seismicity has been reported in only a few subduction zones
342 around the world besides the Antilles, namely, NE Japan, New Zealand, Columbia and
343 Greece. Such events have been attributed to the deformation of subducted seamounts
344 (Uchida *et al.*, 2010), or hydraulic fracturing/fluid-assisted embrittlement or weakening
345 due to the ascent of fluids from the slab (Chang *et al.*, 2017, Halpaap *et al.*, 2019). If
346 this is the case for the Lesser Antilles, then the mantle wedge earthquakes may
347 represent an unusual pathway for fluids driven off by early metamorphic reactions in the
348 subducting plate. Alternatively, in a mantle wedge of mixed chemical composition
349 (Laigle *et al.*, 2013), preferential hydration of the peridotite components may result in a
350 differential volume change that may open fractures, causing extensional faulting in the
351 mantle wedge (Iyer *et al.*, 2008).

352

353 **Plate Interface Seismicity**

354 In the north, interplate seismicity is observed from depths of about 10 km, while in the
355 south, the shallowest seismicity is at 30 km depth at 14°N, and 45 km south of 12°N

356 (profiles in Figure 5). The largest thrust earthquake (M_w 5.8) on the plate interface
357 during our deployment occurred on 3 February 2017 east of Martinique. The Martinique
358 earthquake was followed by aftershocks at ~ 50 km depth (profile C-C'). We relocated
359 the M_w 5.8 mainshock to 51 km depth. The alignment of the sequence with the slab
360 geometry indicates rupture of the plate interface and suggests a seismogenic zone
361 reaching to at least 60 km depth, deeper than the fault locking depth of 5-25 km
362 previously proposed by Smithe *et al.* (2015) using geodetic observations.

363
364 The Martinique sequence occurred deeper than the intersection of the upper plate Moho
365 (~ 27 km) with the down-going plate interface. This observation is similar to that found by
366 Ruiz *et al.* (2013) of seismic activity offshore Martinique and Dominica, suggesting that
367 the interplate seismogenic zone width is usually not limited by thickness of the upper
368 plate crust, consistent with a global compilation by Heuret *et al.* (2011). However, the
369 down-dip limit of ~ 65 km depth that we find for the Lesser Antilles megathrust
370 seismogenic zone is high compared to the global range of 51 ± 8 km (Heuret *et al.*,
371 2011). The Martinique sequence on the plate interface, together with supra-slab
372 seismicity discussed in the previous section, suggest the existence of a cold mantle
373 nose, which can effectively extend the decoupling depth of the slab and upper plate
374 mantle (Wada and Wang, 2009). This wide seismogenic zone has important
375 implications for the maximum magnitude of earthquakes that could occur in this region,
376 and this may explain the large magnitudes of the Guadeloupe earthquakes in the
377 1800s. An alternative to this is that this deeper part may represent seismic-aseismic
378 transitional zone (e.g., Lay et al., 2012). Although large earthquakes may not initiate at
379 this deeper depth, rupture may propagate into this region and effectively increase the
380 earthquake magnitude and thus seismic hazard.

381

382 **Intermediate Depth Seismicity**

383 The Lesser Antilles Wadati-Benioff zone extends to 150-180 km depth with a
384 concentration of intraslab seismicity beneath the center of the arc, between the islands
385 of Guadeloupe and St. Lucia (Figure 5). During our experiment, a M_w 5.6 earthquake
386 occurred on 18 October 2016 southwest of Dominica at ~ 160 km depth. This event had

387 a normal faulting mechanism with both nodal planes striking perpendicular to the arc,
388 and in the direction of convergence. Normal faulting earthquakes are frequent within the
389 slab at ~150 km depth between the islands of Dominica and Martinique, i.e. in the
390 region with the densest intermediate depth seismicity. Similar recent moderate-to-large
391 intraplate events (Figure 6) include a M_w 5.6 on 28 December 2015, a M_w 7.4 on 29
392 November 2007, and a M_w 5.8 on 24 September 1996 and an earlier magnitude 7.5 that
393 occurred on 19 March 1953 (Stein *et al.*, 1983) ~100 km south of the 2016 event.
394 According to the GCMT earthquake catalogue, all those events since the 1990s share a
395 similar, normal faulting mechanism with a minor strike-slip component; at least one of
396 the nodal planes strikes parallel with the subduction direction.

397
398 Fault strikes parallel or oblique to the trench could be due to reactivation of subducted
399 outer-rise normal faults formed at the mid-oceanic spreading ridge (e.g., Delouis and
400 Legrand, 2007; Garth and Rietbrock, 2014). However, trench-perpendicular nodal plane
401 ruptures cannot be explained in this manner. Instead, the intermediate-depth normal
402 fault earthquakes mentioned above occurred around the projected positions of the
403 subducted Marathon and Mercurius Fracture zones (Figure 6). This finding may suggest
404 a link between the deep normal fault earthquakes and subducted fracture zones – which
405 may be effective vessels to bring water to intermediate depths. Thus, the reactivation of
406 inherited oceanic structures (e.g., fractures zones), facilitated by dehydration
407 embrittlement, may be the dominant mechanism responsible for the normal faulting
408 events seen at intermediate depth in the central arc. In other places along the arc,
409 intermediate depth normal fault earthquakes are rare, which may suggest weaker
410 hydration and smaller fluid fluxes, insufficient to drive significant dehydration
411 embrittlement failure.

412

413 **Slab Tear?**

414 The coherent catalogue of seismicity compiled for this study offers a chance to test the
415 hypothesis that a slab tear exists at 15°N - between the islands of Dominica and
416 Martinique – as suggested by teleseismic tomography models and seismic anisotropy
417 observations (Van Benthem *et al.*, 2013; Harris *et al.*, 2018; Schlaphorst *et al.*, 2017).

418 We projected seismicity in this area onto multiple profiles (with a 10 km gap between
419 neighbouring profiles) perpendicular to the trench and marked those to the north of the
420 profile in blue, and those to the south in red (Figure S6). This method can reveal the
421 location of a slab tear, if two seismicity alignments with different dip angles are
422 observed. Our results do not indicate any distinctive change in dip angle but rather a
423 thickening of the Wadati-Benioff zone from north to south as shown by line 7 in Figure
424 S6. The thickening here may define the northern boundary of the subducted Marathon
425 Fracture zone. Seismicity during the period of our observation does not support the
426 notion that a large-scale slab tear exists at this depth, but we cannot rule out a slab tear
427 below the deepest seismicity.

428

429 **CONCLUSIONS**

430

431 In this study, we used seismic data from a dense OBS network to record local seismicity
432 in the Lesser Antilles subduction zone and delineate changes in seismic deformation
433 and velocity structure both with depth and along the arc. The joint inversion for a 1-D
434 velocity model, earthquake location and station corrections yields an optimal crustal
435 thickness of 27 km, representative of an arc-back-arc average. Abundant intermediate-
436 depth seismicity is found beneath the islands of Martinique and Dominica, which may
437 relate to the subducted Marathon and Mercurius Fracture Zones. Although a slab tear
438 near 15°N has been proposed by previous teleseismic seismic studies, our seismicity
439 distribution suggests thickening of the Wadat-Benioff zone, but without distinctive
440 changes in the slab dip angle that would be expected for a tear. Interpretations of our
441 earthquake locations reveal pervasive seismicity in the cold mantle wedge corner, which
442 is not observed in many subduction zones. Together with the deep 2016 Martinique
443 earthquake sequence on the plate interface, these observations suggest an abnormally
444 cold and, therefore, wide megathrust seismogenic zone reaching ~65 km depth. It is
445 worth to further investigate whether these features are inherent to the slow subduction
446 of slow-spreading oceanic lithosphere in the Atlantic. These results provide a new
447 framework for advances in operational earthquake locations and future estimation of
448 seismic hazard in the Eastern Caribbean.

449

450 **DATA AND RESOURCES**

451 The optimal 1-D velocity model is made available in the electronic supplement to this
452 article (Table S1). The relocated earthquake catalogue is available in Table S2. The
453 Global Centroid Moment Tensor Project database was searched using
454 www.globalcmt.org/CMTsearch.html (last accessed on April 1, 2019). We made figures
455 using GMT (Wessel and Smalley, 1998). Supplemental content for this article includes
456 figures showing the quality of earthquake magnitude estimation, the relationship
457 between station correction and elevation, the comparison of our slab geometry with that
458 of Slab2.0, and seismicity projected to dense profiles in the central part of the arc.

459

460

461 **ACKNOWLEDGEMENTS**

462 This work was funded under NERC grant NE/K010611/1. We thank the “German
463 Instrument Pool for Amphibian Seismology (DEPAS)”, hosted by the Alfred Wegener
464 Institute Bremerhaven, for providing the ocean-bottom seismometers and temporary
465 island seismometers, and UCSD (Scripps) for providing additional ocean-bottom
466 seismometers. We thank Allison Bent, Zhigang Peng, Hongfeng Yang, and two
467 anonymous reviewers for their helpful and constructive comments.

468

469 **REFERENCES**

470

471 Allen, R., J. Collier, T. Henstock, A. Stewart, and S. Goes, 2019, A new tectonic model
472 for the Lesser Antilles: Evidence for a buried arc in the eastern Caribbean, *Geophysical*
473 *Research Abstract*, 21, EGU2019-7944

474

475 Bakun, W. H., and W. B., Joyner (1984), The ML scale in central California, *Bull.*
476 *Seismol. Soc. Am.*, 74(5), 1827-1843.

477

478 Bie, L., T. Garth, and A. Rietbrock, 2017, Links between the distribution of intermediate
479 depth seismicity and structure of the incoming plate in the Lesser Antilles arc, In AGU
480 Fall Meeting Abstracts. #T31D-0672

481

482 Abers, G. A., P. E. van Keken, E. A. Kneller, A. Ferris, and J. C. Stachnik (2006), The
483 thermal structure of subduction zones constrained by seismic imaging: Implications for
484 slab dehydration and wedge flow, *Earth Planet. Sci. Lett.*, 241(3-4), 387-397.

485

486 Bazin, S., N. Feuillet, C. Duclos, W. Crawford, A. Nercessian, M. Bengoubou-Valérius,
487 et al., (2010), The 2004–2005 Les Saintes (French West Indies) seismic aftershock
488 sequence observed with ocean bottom seismometers, *Tectonophysics*, 489(1-4), 91-
489 103.

490

491 Bird, P. (2003), An updated digital model of plate boundaries, *Geochem. Geophys.*
492 *Geosyst.*, 4(3), 1027, doi:10.1029/2001GC000252.

493

494 Boynton, C. H., G. K. Westbrook, M. H. P. Bott, and R. E. Long (1979), A seismic
495 refraction investigation of crustal structure beneath the Lesser Antilles island arc,
496 *Geophys. J. R. Astron. Soc.*, 58, 371–393.

497

498 Chang, Y., L. M. Warren, and G. A. Prieto (2017), Precise Locations for Intermediate-
499 Depth Earthquakes in the Cauca Cluster, Colombia, *Bull. Seismol. Soc. Am.*, 107(6),
500 2649-2663.

501

502 Delouis, B., and D. Legrand (2007), Mw 7.8 Tarapaca intermediate depth earthquake of
503 13 June 2005 (northern Chile): Fault plane identification and slip distribution by
504 waveform inversion, *Geophys. Res. Lett.*, 34(1).

505

506 DeMets, C., R. G. Gordon, and D. F. Argus (2010), Geologically current plate motions,
507 *Geophys. J. Int.*, 181, 1–80.

508

509 Dorel, J. (1981), Seismicity and seismic gap in the Lesser Antilles arc and earthquake
510 hazard in Guadeloupe, *Geophys. J. R. Astron. Soc.*, 67(3), 679-695.

511

512 Eberhart-Phillips, D. (1990), Three-dimensional P and S velocity structure in the
513 Coalinga region, California. *J. Geophys. Res.*, 95(B10), 15343-15363.

514

515 Escartín, J., D. K. Smith, J. Cann, H. Schouten, C. H. Langmuir, and S. Escrig (2008),
516 Central role of detachment faults in accretion of slow-spreading oceanic
517 lithosphere, *Nature*, 455(7214), 790.
518

519 Feuillet, N., F. Beauducel, and P. Tapponnier (2011), Tectonic context of moderate to
520 large historical earthquakes in the Lesser Antilles and mechanical coupling with
521 volcanoes, *J. Geophys. Res.*, 116(B10), doi:10.1029/2011JB008443
522

523 Garth, T., and A. Rietbrock (2014), Downdip velocity changes in subducted oceanic
524 crust beneath Northern Japan-insights from guided waves, *Geophys. J. Int.*, 198(3),
525 1342-1358. doi:10.1093/gji/ggu206
526

527 González, O., V. Clouard, and J. Zahradnik (2017), Moment tensor solutions along the
528 central Lesser Antilles using regional broadband stations, *Tectonophysics*, 717, 214-
529 225.
530

531 González, O., V. Clouard, S. Tait, and G. F. Panza (2018), S-wave velocities of the
532 lithosphere-asthenosphere system in the Lesser Antilles from the joint inversion of
533 surface wave dispersion and receiver function analysis, *Tectonophysics*, 734, 1-15.
534

535 Halpaap, F., S. Rondenay, A. Perrin, S. Goes, L. Ottemöller, H. Austrheim, R. Shaw,
536 and T. Eeken (2019), Earthquakes track subduction fluids from slab source to mantle
537 wedge sink, *Sci. Adv.*, 5(4), DOI: 10.1126/sciadv.aav7369.
538

539 Harris, C. W., M. S. Miller, and R. W. Porritt (2018), Tomographic Imaging of Slab
540 Segmentation and Deformation in the Greater Antilles, *Geochem. Geophys. Geosyst.*,
541

542 Hayes, G. P., D. E. McNamara, L. Seidman, and J. Roger (2013), Quantifying potential
543 earthquake and tsunami hazard in the Lesser Antilles subduction zone of the Caribbean
544 region, *Geophys. J. Int.*, 196(1), 510-521.
545

546 Hayes, G. P., G. L. Moore, D. E. Portner, M. Hearne, H. Flamme, M. Furtney, and G. M.
547 Smoczyk (2018), Slab2, a comprehensive subduction zone geometry
548 model, *Science*, 362(6410), 58-61.
549

550 Heuret, A., C. P. Conrad, F. Funiciello, S. Lallemand, and L. Sandri (2012), Relation
551 between subduction megathrust earthquakes, trench sediment thickness and upper
552 plate strain, *Geophys. Res. Lett.*, 39(5).
553

554 Heuret, A., S. Lallemand, F. Funiciello, C. Piromallo, and C. Faccenna (2011), Physical
555 characteristics of subduction interface type seismogenic zones revisited, *Geochem.*
556 *Geophys. Geosyst.*, 12(1).
557

558 Hicks, S., A. Rietbrock, I. Ryder, C. Lee, and M. Miller (2004), Anatomy of a megathrust:
559 The 2010 M8.8 Maule, Chile earthquake rupture zone imaged using seismic
560 tomography, *Earth Planet. Sci. Lett.*, 405, 142-155, doi.org/10.1016/j.epsl.2014.08.028

561
562 Husen, S., E. Kissling, E. Flueh, and G. Asch (1999), Accurate hypocentre
563 determination in the seismogenic zone of the subducting Nazca Plate in northern Chile
564 using a combined on/offshore network, *Geophys. J. Int.*, 138(3), 687-701.
565
566 Iyer, K., B. Jamtveit, J. Mathiesen, A. Malthe-Sørenssen, and J. Feder (2008),
567 Reaction-assisted hierarchical fracturing during serpentinization, *Earth Planet. Sci. Lett.*,
568 267(3-4), 503-516.
569
570 Kennett B. L. N., and E. R. Engdahl (1991), Travel times for global earthquake location
571 and phase association, *Geophys. J. Int.*, 105, 429-465.
572
573 Kissling, E., W. L. Ellsworth, D. Eberhart-Phillips, and U. Kradolfer (1994), Initial
574 reference models in local earthquake tomography, *J. Geophys. Res.*, 99, 19,635–
575 19,646, doi:10.1029/93JB03138.
576
577 Kissling, E. (1988), Geotomography with local earthquake data, *Rev. Geophys.*, 26(4),
578 659-698.
579
580 Laigle, M., A. Hirn, M. Sapin, A. Bécel, P. Charvis, E. Flueh, et al., (2013), Seismic
581 structure and activity of the north-central Lesser Antilles subduction zone from an
582 integrated approach: Similarities with the Tohoku forearc, *Tectonophysics*, 603, 1-20.
583
584 Lay, T., H. Kanamori, C. J. Ammon, K. D. Koper, A. R. Hutko, L. Ye, H. Yue, and T. M.
585 Rushing (2012), Depth-varying rupture properties of subduction zone megathrust
586 faults. *J. Geophys. Res.*, 117(B4311), doi:10.1029/2011JB009133.
587
588 López, A. M., S. Stein, T. Dixon, G. Sella, E. Calais, P. Jansma, Weber, and P.
589 LaFemina (2006), Is there a northern Lesser Antilles forearc block?, *Geophys. Res.*
590 *Lett.*, 33(7).
591
592 McCann, W. R., and L. R. Sykes (1984), Subduction of aseismic ridges beneath the
593 Caribbean plate: Implications for the tectonics and seismic potential of the northeastern
594 Caribbean, *J. Geophys. Res.*, 89(B6), 4493-4519.
595
596 McKenzie, D., J. Jackson, and K. Priestley (2005), Thermal structure of oceanic and
597 continental lithosphere, *Earth Planet. Sci. Lett.*, 233(3-4), 337-349.
598
599 Nippres, S. E. J., A. Rietbrock, and A. E. Heath (2010), Optimized automatic pickers:
600 application to the ANCORP data set. *Geophys. J. Int.*, 181(2), 911-925.
601
602 Paulatto, M., M. Laigle, A. Galve, P. Charvis, M. Sapin, G. Bayrakci, ... and H. Kopp
603 (2017), Dehydration of subducting slow-spread oceanic lithosphere in the Lesser
604 Antilles, *Nat. Comm.*, 8, 15980.
605

606 Raffaele, R. M. (2011), Seismic structure of subduction zone of the Lesser Antilles, PhD
607 thesis, University of Catania.
608

609 Rietbrock, A., I. Ryder, G. Hayes, C. Haberland, D. Comte, S. Roecker, and H. Lyon-
610 Caen (2012), Aftershock seismicity of the 2010 Maule Mw8.8, Chile, earthquake:
611 Correlation between co-seismic slip models and aftershock distribution? *Geophys. Res.*
612 *Lett.*, 39(8). doi:10.1029/2012GL051308.
613

614 Ruiz, M., A. Galve, T. Monfret, M. Sapin, P. Charvis, M. Laigle, ... and J. Diaz (2013),
615 Seismic activity offshore Martinique and Dominica islands (Central Lesser Antilles
616 subduction zone) from temporary onshore and offshore seismic networks,
617 *Tectonophysics*, 603, 68-78.
618

619 Goes, S., et al. (2019), Project VoiLA: Volatile Recycling in the Lesser Antilles, *Eos*,
620 100, <https://doi.org/10.1029/2019EO117309>.
621

622 Schlaphorst, D., J. M. Kendall, J. S. Collier, J. P. Verdon, J. Blundy, B. Baptie, ... and M.
623 P. Bouin (2016), Water, oceanic fracture zones and the lubrication of subducting plate
624 boundaries—insights from seismicity, *Geophys. J. Int.*, 204(3), 1405-1420.
625

626 Schlaphorst, D., J. M. Kendall, B. Baptie, J. L. Latchman, and S. Tait (2017), Gaps,
627 tears and seismic anisotropy around the subducting slabs of the Antilles,
628 *Tectonophysics*, 698, 65-78.
629

630 Stein, S., J. F. Engeln, D. A. Wiens, R. C. Speed, and K. Fujita (1983), Slow subduction
631 of old lithosphere in the Lesser Antilles, *Tectonophysics*, 99(2-4), 139-148.
632

633 Symithe, S., E. Calais, J. B. De Chabaliere, R. Robertson, and M. Higgins (2015),
634 Current block motions and strain accumulation on active faults in the Caribbean, *J.*
635 *Geophys. Res.*, 120(5), 3748-3774.
636

637 Thurber, C. H. (1992), Hypocenter-velocity structure coupling in local earthquake
638 tomography, *Phys. Earth Planet. In.*, 75(1-3), 55-62.
639

640 Uchida, N., S. H. Kirby, T. Okada, R. Hino, and A. Hasegawa (2010), Supraslab
641 earthquake clusters above the subduction plate boundary offshore Sanriku,
642 northeastern Japan: Seismogenesis in a graveyard of detached seamounts?, *J.*
643 *Geophys. Res.*, 115(B9).
644

645 van Benthem, S., R. Govers, W. Spakman, and R. Wortel (2013), Tectonic evolution
646 and mantle structure of the Caribbean, *J. Geophys. Res.*, 118(6), 3019-3036.
647

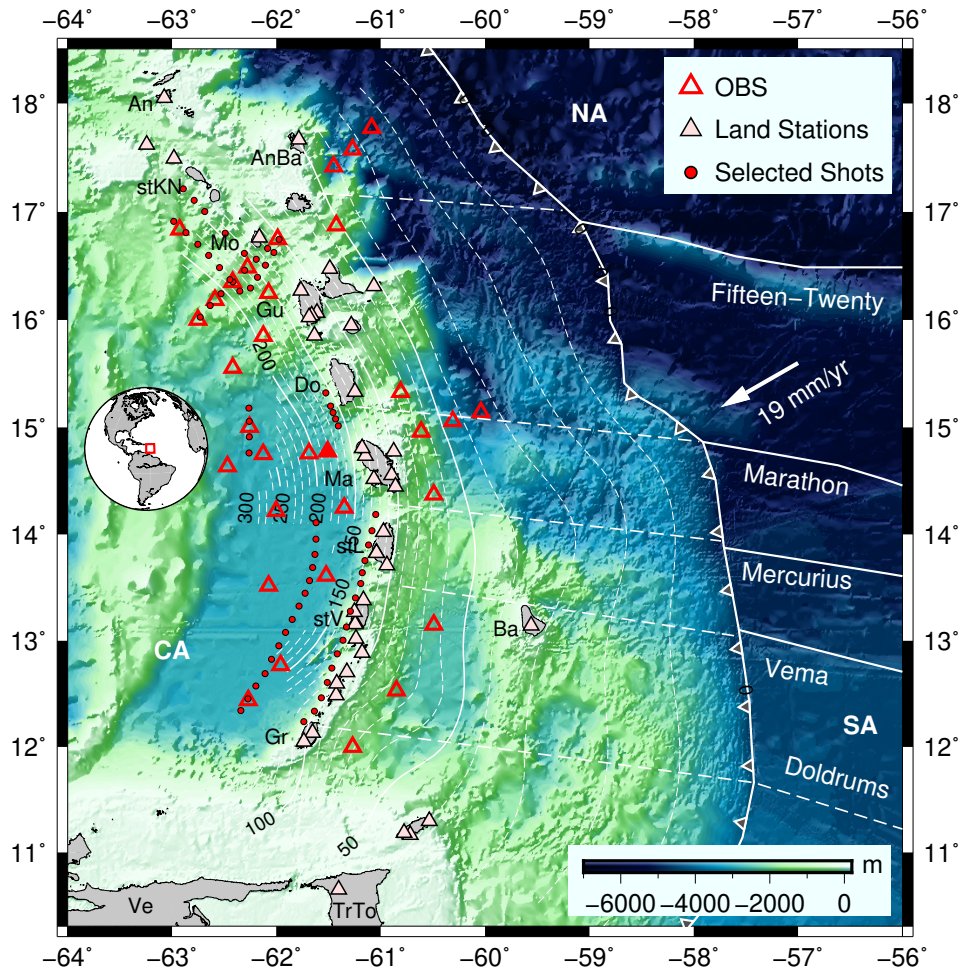
648 Wada, I., and K. Wang (2009), Common depth of slab-mantle decoupling: Reconciling
649 diversity and uniformity of subduction zones, *Geochem. Geophys. Geosyst.*, 10(10).
650

651 Wadge, G., and J. B. Shepherd (1984). Segmentation of the Lesser Antilles subduction
652 zone, *Earth Planet. Sci. Lett.*, 71(2), 297-304.
653
654 Weber, J. C., H. Geirsson, J. L. Latchman, K. Shaw, P. La Femina, S. Wdowinski, et al.,
655 (2015), Tectonic inversion in the Caribbean-South American plate boundary: GPS
656 geodesy, seismology, and tectonics of the Mw 6.7 22 April 1997 Tobago earthquake,
657 *Tectonics*, 34(6), 1181-1194.
658
659 Wessel, P., and R. Smalley (1998). New, improved version of generic mapping tools
660 released, *Eos Trans. AGU* 79, no. 47, 579-579.
661
662 Zhu, G., H. Yang, J. Lin, Z. Zhou, M. Xu, J. Sun, and K. Wan (2019), Along-strike
663 variation in slab geometry at the southern Mariana subduction zone revealed by
664 seismicity through ocean bottom seismic experiments, *Geophys. J. Int.*, 218(3), 2122-
665 2135, doi:10.1093/gji/ggz272.

666 *Lidong Bie*
667 *Andreas Rietbrock*
668 *Geophysical Institute, Karlsruhe Institute of Technology, Germany*
669 *Department of Earth Ocean & Ecological Sciences, University of Liverpool, UK*
670 [*l.bie@liv.ac.uk*](mailto:l.bie@liv.ac.uk)
671
672 *Stephen Hicks*
673 *Robert Allen*
674 *Jenny Collier*
675 *Saskia Goes*
676 *Department of Earth Science & Engineering, Imperial College London, UK*
677
678 *Jon Blundy*
679 *Mike Kendall*
680 *School of Earth Sciences, University of Bristol, UK*
681
682 *Nick Harmon*
683 *Tim Henstock*
684 *Kate Rychert*
685 *Department of Ocean & Earth Sciences, University of Southampton, UK*
686
687 *Jon Davidson(Deceased)*
688 *Colin Macpherson*
689 *Jeroen van Hunen*
690 *Department of Earth Sciences, University of Durham, UK*
691
692 *Valerie Clouard*
693 *Stephen Tait*
694 *Institut de Physique du Globe de Paris, Université Paris Diderot, France*
695
696 *Thomas Garth*

697 *Department of Earth Sciences, University of Oxford, UK*
698
699 *Lloyd Lynch*
700 *Richard Robertson*
701 *Seismic Research Centre, The University of the West Indies, Trinidad and Tobago*
702
703 *Frank Krüger*
704 *Institute of Geosciences, University of Potsdam, Germany*
705
706 *Jamie Wilkinson*
707 *Natural History Museum, London, UK*
708
709 *Marjorie Wilson*
710 *School of Earth & Environment, University of Leeds*
711

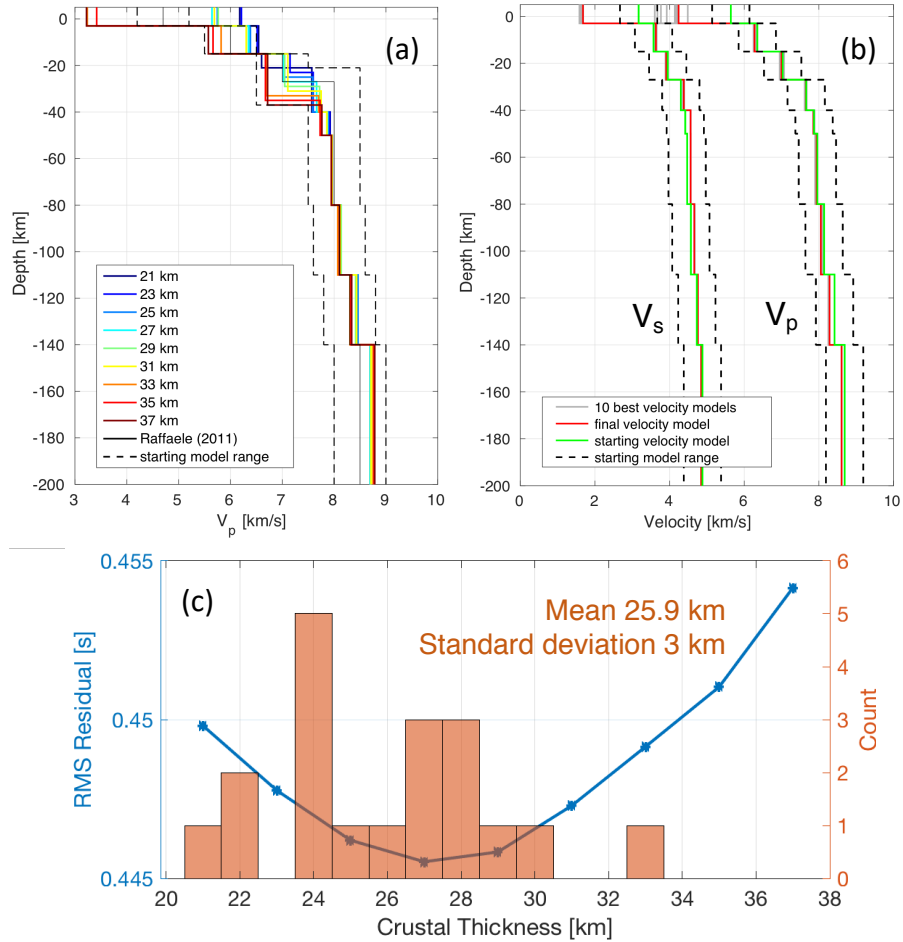
712
713



714
715

716 Figure 1. Tectonic map of the Lesser Antilles subduction zone. Offshore and onshore
717 seismic stations used in this study are marked by empty red and filled triangles,
718 respectively. Light white contours depict refined slab geometry from this study.
719 Reference station in the 1-D velocity inversion is filled by red colour. Red dots in the
720 back-arc indicate active shots included in the inversion. Details of land stations
721 incorporated in this study are shown in Figure S1. Inferred fracture zone and spreading-
722 ridge structures (Schlaphorst *et al.*, 2016) are shown with white lines. CA: Caribbean
723 Plate; NA: North American Plate; SA: South American Plate. See Figure S1 for details
724 of island name abbreviations.

725



726

727 Figure 2. (a) Best v_p models for simulations with different starting velocity layer
 728 configuration. The crustal thickness is varied from 21 km to 37 km, in 2 km increments.

729 (b) Final v_p and v_s models for the Lesser Antilles subduction zone. (c) RMS residual
 730 versus the tested crustal thickness. The minimum RMS misfit is achieved with a crustal
 731 thickness of 27 km. The bar chart shows the distribution of crustal thickness derived by
 732 González et al. (2018) from 19 land stations along the arc.

733

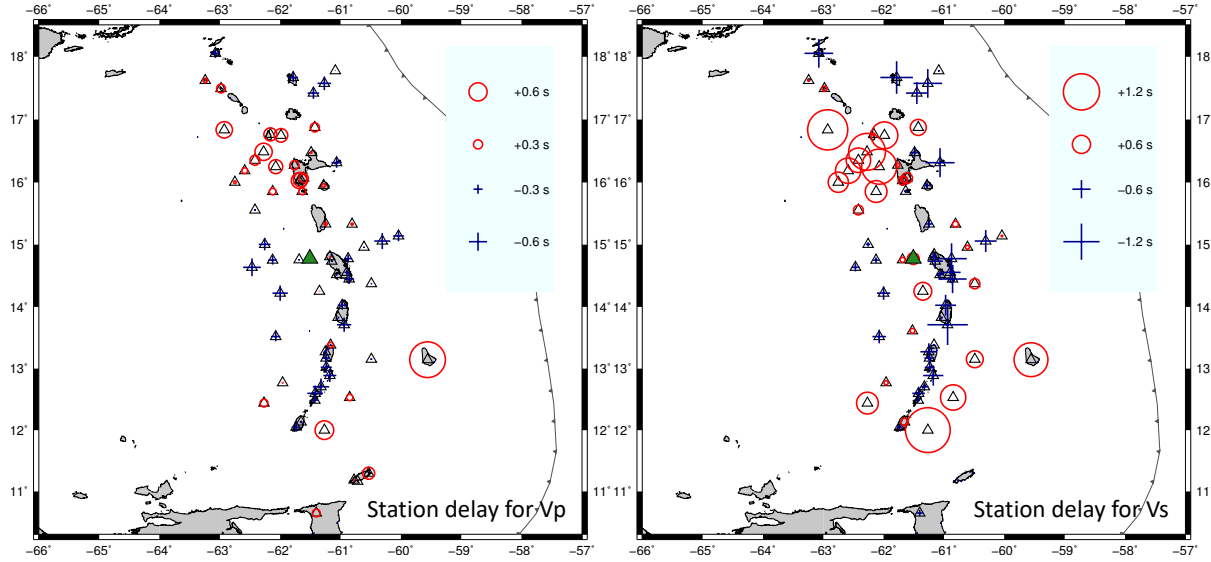
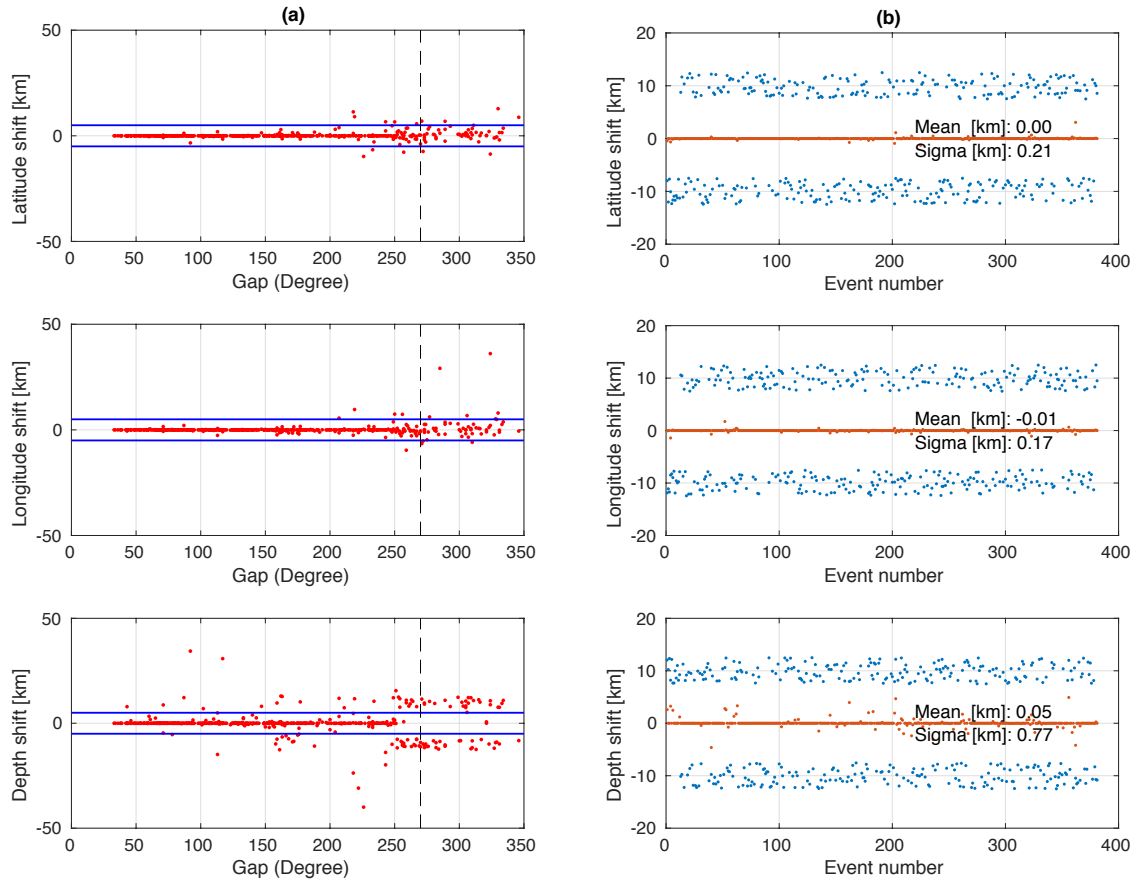
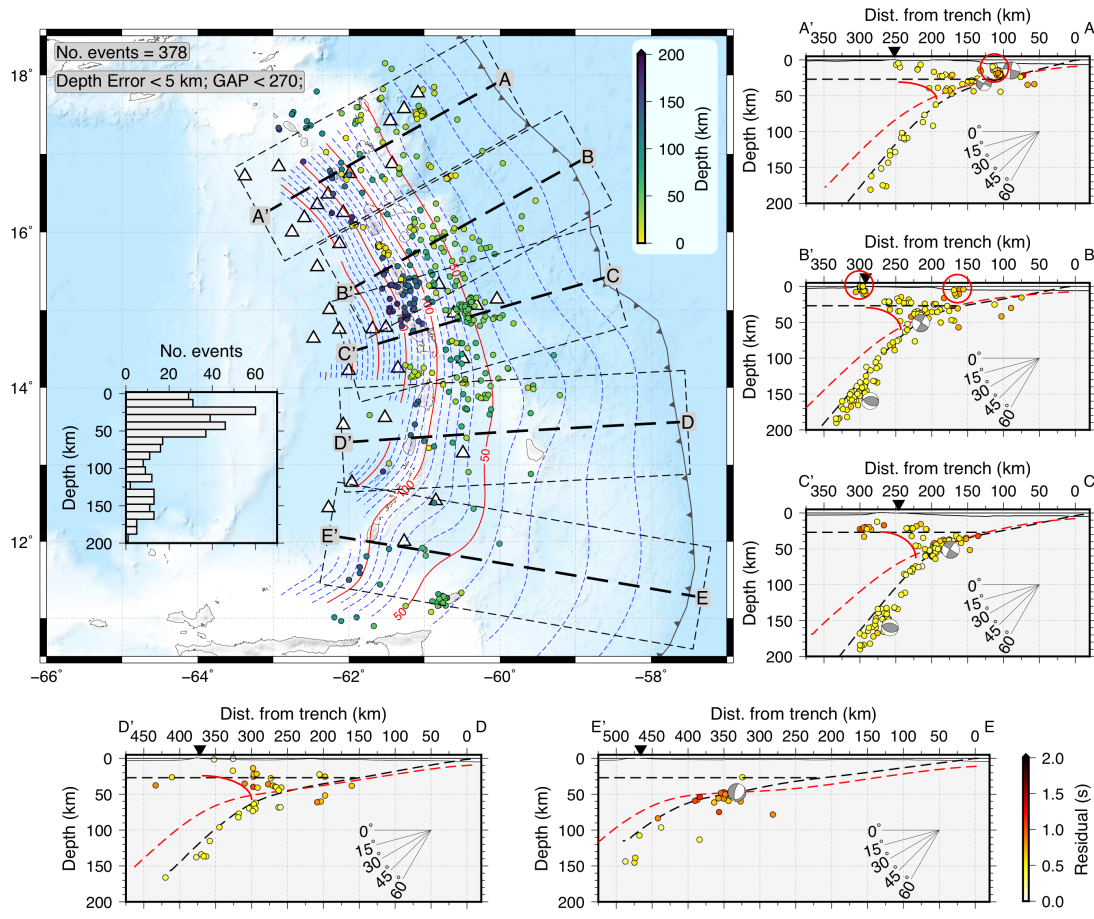


Figure 3. Station corrections associated with the velocity model shown in Figure 2b.



737

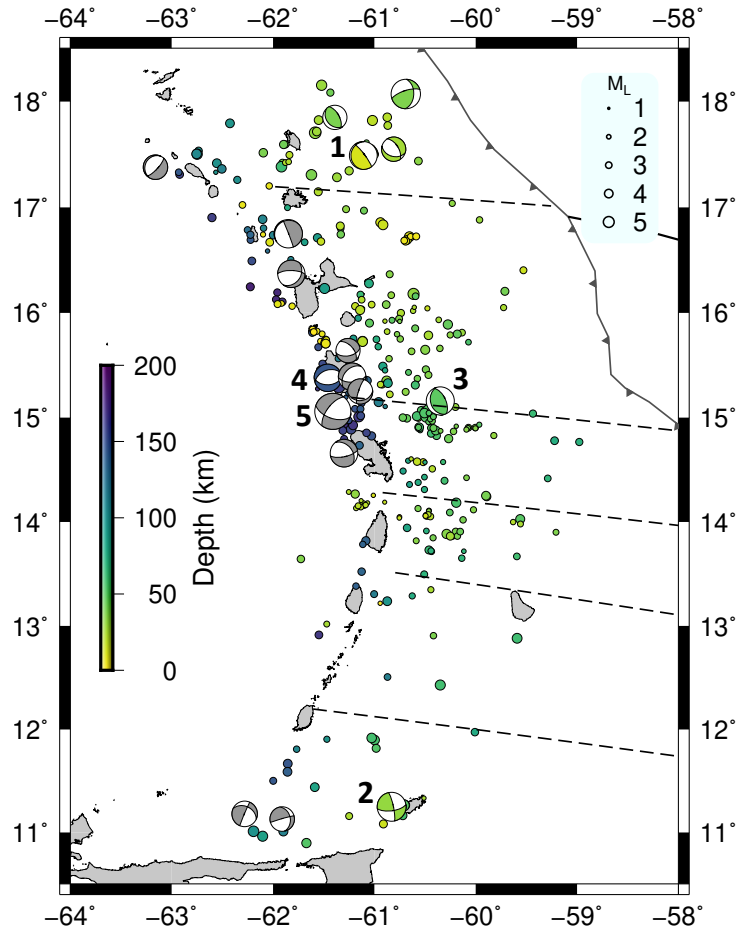
738 Figure 4. Stability test using the velocity model shown in Figure 2b to recover the
 739 randomly perturbed earthquakes (blue points) in the longitude, latitude and depth
 740 directions. Those recovered (red points) to be within 5 km (marked as blue line in the
 741 left panels) from their original locations and having azimuthal gap smaller than 270°
 742 (black dashed line) are deemed as events with good quality and shown in Figure 5 and
 743 6. The panels on the right side show the mean and standard deviation of the difference
 744 between the recovered (red points) and perturbed (blue points) earthquake locations in
 745 three directions for good quality events.



746
 747
 748
 749
 750
 751
 752
 753
 754
 755
 756
 757
 758
 759

Figure 5. Distribution of the relocated 378 events coloured by hypocentral depth. The inset shows the number of events versus depth. Triangles are the stations from the VoiLA OBS deployment. Dashed blue and red lines represent the refined slab geometry from this study. Red curve delineates the wedge-shaped mantle corner seismicity. Depth profiles through the regional events comprise earthquakes that are within 75 km perpendicular distance of the labelled lines on the map. In the profiles, earthquakes are coloured by their RMS misfit after the relocation using the best 1-D velocity models from this study. The side hemisphere focal mechanisms from the Global Centroid Moment Tensor Project (see Data and Resources) are plotted. Black dashed curves are from slab model generated in this study, while the red dashed curves are from Slab2.0 (Hayes et al., 2018).

760



761

762 Figure 6. Local seismicity as derived from this study. Focal mechanisms (FM) for events
763 with GCMT (see Data and Resources) solutions during the period of passive-seismic
764 experiments are coloured by depth. Focal mechanisms for all historical deep (> 70 km)
765 normal fault events (at least one slip direction between -145° and -90°) in the GCMT
766 catalogue and from Gonzalez et al. (2017) are marked in grey. FM 1: M_w 5.7,
767 2017/04/17; FM 2: M_w 5.9, 2016/12/06; FM 3: M_w 5.8, 2017/02/03; FM 4: M_w 5.6,
768 2016/10/18; FM 5: M_w 7.4, 2007/11/29.

769